



Research on waterproofing and drainage optimization scheme for karst tunnel lining in water-rich areas

Dongping Zhao^{1,2} · Haobo Fan³ · Lingli Jia⁴ · Yuxiang Song³

Received: 5 December 2019 / Accepted: 30 September 2020 / Published online: 8 February 2021
© The Author(s), under exclusive licence to Springer-Verlag GmbH, DE part of Springer Nature 2021

Abstract

In the presence of heavy rainfall on the earth's surface, a series of water-induced problems often appear in karst tunnels, such as lining cracks and invert uplift. An effective method of alleviating these problems is the adjustment of the tunnel drainage scheme. In this study, three waterproofing and drainage optimization schemes were studied using numerical simulation and model tests. Numerical results show that, when the conventional waterproofing and drainage scheme is adopted in water-rich karst tunnels, the water pressure at the tunnel invert cannot be effectively reduced by the drainage system. When the water head height of the tunnel crown is 50 m and the distance between circumferential drainage blind pipes is reduced from 5 to 2 m, the rate of water pressure reduction at the invert from 21 to 27%. When a longitudinal drainage blind pipe is added at the bottom of the invert, the rate of reduction is increased to 84%; however, it is increased to 96% when the central drainage ditch is set at the bottom of the invert. Therefore, placing the central drainage ditch at the bottom of the invert has the most significant effect on reducing the water pressure. Model test results indicate that when the water head height of the tunnel crown is 12 m, the reduction rates of water pressure at the invert corresponding to the placement of a central drainage ditch at the bottom of the invert are 66%. The model test results were found to be consistent with numerical results.

Keywords Rich water · Karst tunnel · Lining · Water pressure · Optimized drainage scheme

Introduction

By the end of 2018, there were 15,117 railway tunnels in operation in China, with a cumulative length of 16,331 km (Zhao and Tian 2019; Zhao et al. 2017), and the total number of tunnels in operation estimated to reach 17,000 by the end of 2020. In the field of tunnel engineering, China has already become a world leader. In terms of conventional mountain tunnels, China has accumulated rich experience

in construction, whereas in terms of karst tunnels, there are still many technical problems to be further improved.

China has widest karst distribution area in the world (about 20% of the total karst area in the world)—the karst landforms cover many provinces, especially in Guangxi, Yunnan and Guizhou, and several railways cross the karst landforms. For example, the Chengdu-Guiyang Railway, the Chongqing-Lichuan Railway and the Shanghai-Kunming Railway which are already in operation, as well as the Zhengzhou-Wanzhou Railway under construction, all pass through large-scale karst landscapes. Hence, there are numerous karst tunnel projects along the above-mentioned railway lines (Fig. 1). Whether during construction or operation, dealing with groundwater in tunnels is one of the most important issues related to their structural safety in karst regions (Casagrande et al. 2005; Fan et al. 2018). For water-rich karst tunnels, the permeability coefficient of the surrounding rock is relatively large and the water pressure on the tunnel lining is strongly affected by surface water recharge. In the case of continuous heavy rainfall, surface water seeps in rapidly, because the karst pipelines and cracks in the karst area are widely distributed, groundwater

✉ Haobo Fan
739512276@qq.com

¹ School of Civil Engineering, Southwest Jiaotong University, Chengdu 610031, Sichuan, China
² Key Laboratory of Transportation Tunnel Engineering, Ministry of Education, Southwest Jiaotong University, Chengdu 610031, Sichuan, China
³ State Key Laboratory of Mechanical Behavior and System Safety of Traffic Engineering Structures, Shijiazhuang Tiedao University, Shijiazhuang 050043, China
⁴ School of Architecture and Design, Southwest Jiaotong University, Chengdu 610031, Sichuan, China

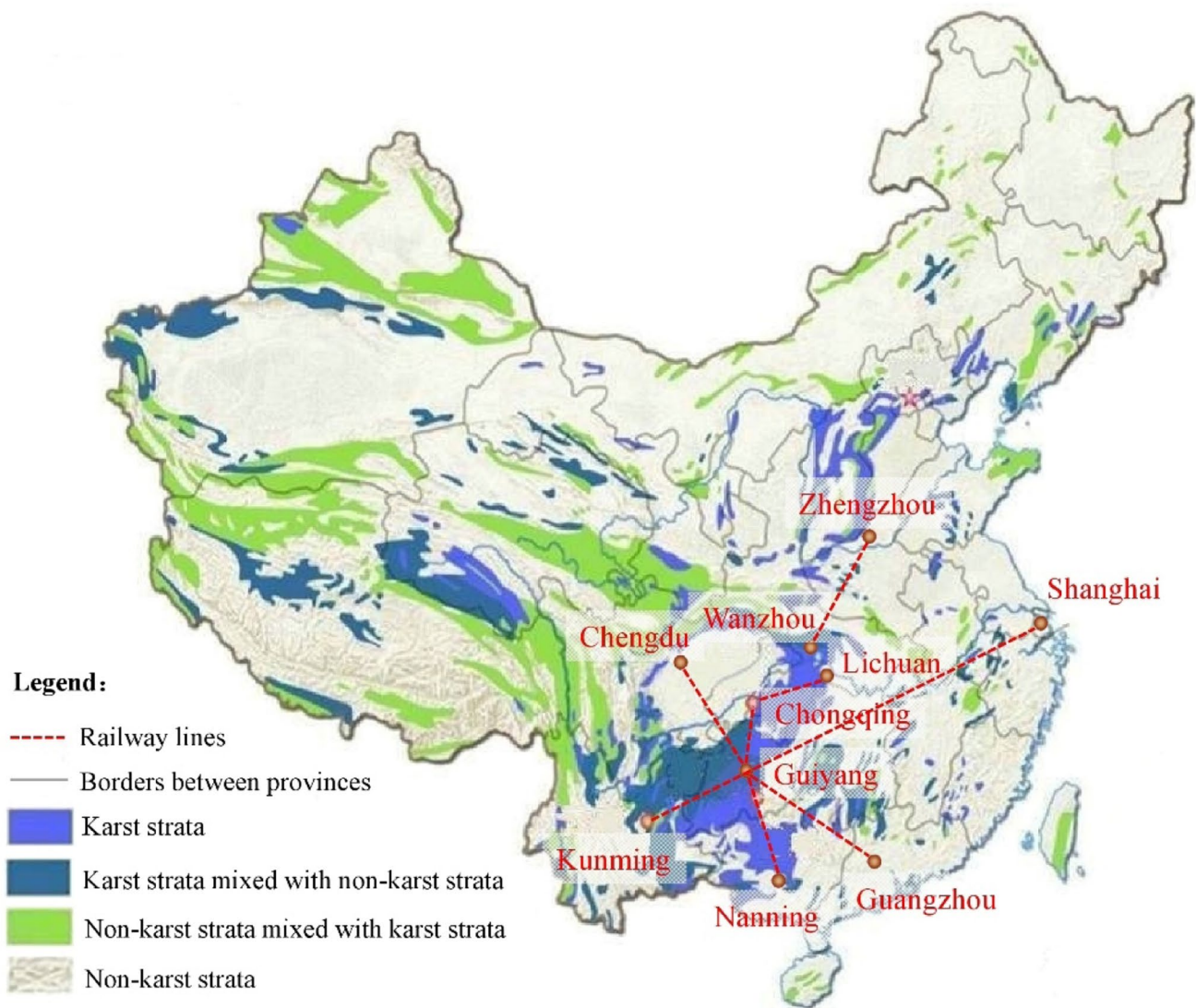


Fig. 1 Karst geomorphology distribution and railway lines crossing karst regions in China

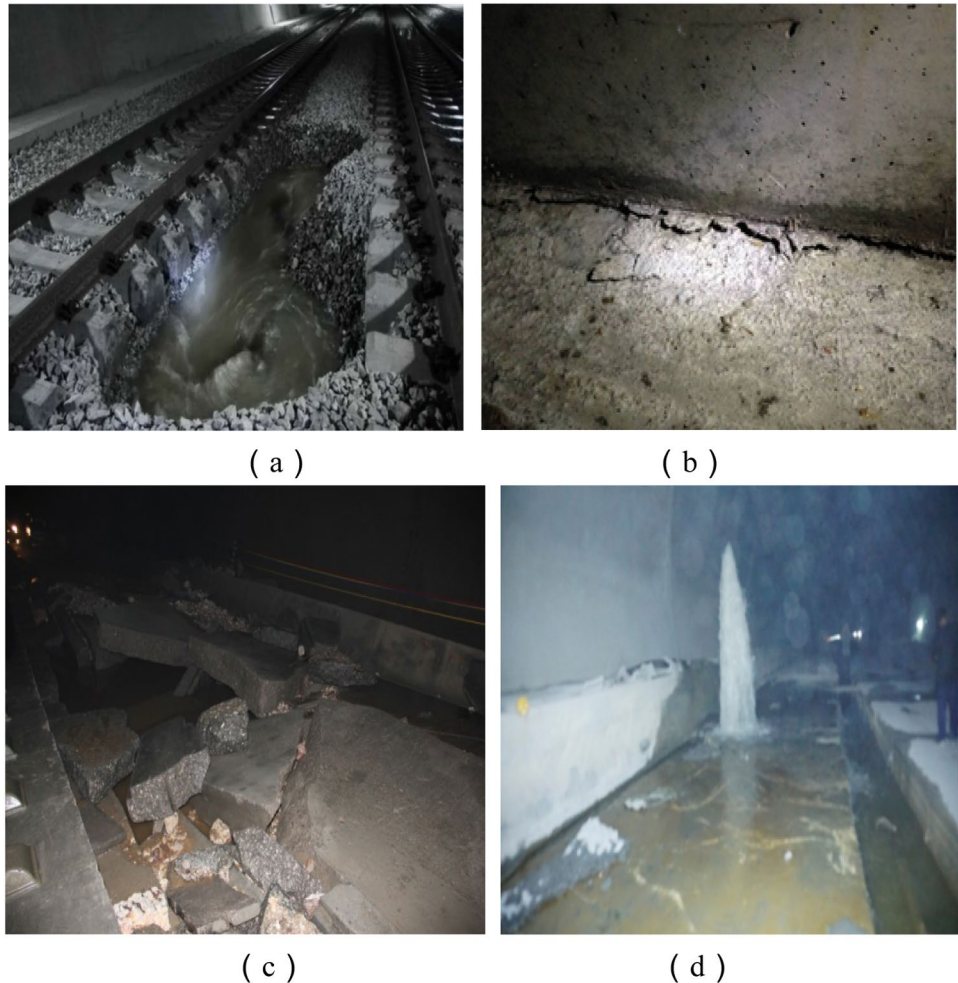
recharge is far greater than the tunnel drainage capacity; therefore, even under drainage conditions, the tunnel lining will bear a large external water pressure, which will endanger the tunnel structure safety (Fu et al. 2007; Yang et al. 2016).

In recent years, there have been many accidents caused by water in karst tunnels that have been opened for operation. For example, the bed slab of the tunnel from Fengdu to Shizhu county in the Chongqing-Lichuan railway was broken by the high water pressure (Fig. 2a). The entire track slab of the Gaotian Tunnel in the Guiyang-Guangzhou railway was separated from the tunnel invert and water pressure indirectly caused deformation of the track in the tunnel (Fig. 2b). Owing to sudden heavy rain, the water pressure on the lining of the small mountain tunnel in the Shanghai-Kunming railway increased rapidly in a short time, eventually

leading to tunnel invert damage (Fig. 2c). Under the action of water pressure, the cracking of the Naji tunnel invert and water gushing occurred in the Kunming-Nanning railway (Fig. 2d).

In previous studies of karst tunnels, problems caused by water during construction have attracted widespread attention in the academic community. Li et al. (2013, 2017a, b, 2019) and Wu et al. (2017) have conducted in-depth research on the problem of water inrush during the construction of karst tunnels, and revealed the mechanism of water inrush in karst tunnels. Jeon et al. (2004) used model tests and numerical simulation methods to study the effects of faults and weak fracture zones on tunnel stability. The influence of fault location and distance between fault and tunnel on lining deformation was obtained. Fang et al. (2016) performed tunnel water pressure model tests and obtained the

Fig. 2 Water hazards in existing karst tunnels: **a** invert broken by high pressure water; **b** track slab was separated from invert; **c** tunnel invert damage; **d** cracking of tunnel invert and water gushing



internal force and failure characteristics of the tunnel lining under undrained conditions; however, their proposed method cannot simulate drainage conditions, as it uses the vacuum method to simulate the water pressure. Tian et al. (2018) developed a test device to study the influence of the relative position relationship between the karst cave and tunnel on the internal forces caused by lining water pressure; the results show that the development of a karst cave affects the tunnel water flow. Nam and Bobet (2006) studied the influence of the water flow on the internal force of the tunnel lining in a water-rich deep-buried tunnel, and analysed the changes in the water pressure behind the lining when the drainage system was not smooth.

Based on the researches presented above, it can be seen that, regarding the construction of water-rich karst tunnels, the existing research focuses on the detection of water bodies, the mechanism of water and mud inrush and on prevention measures during the construction of karst tunnels. In the case of water-rich karst tunnels already in operation, the existing research focuses on the influence

of the smoothness of the tunnel waterproof and drainage system on the lining water pressure. There are only a few reports on water pressure distribution behind the lining of water-rich karst tunnels and improving the water pressure resistance by optimizing the existing waterproof and drainage system.

Base on this, in this study, the water pressure distribution of water-rich karst tunnels was analysed, and optimisation measures for water inrush prevention and drainage were studied. The distribution of water pressure on the lining of karst tunnels was revealed, under the condition that the surface recharge is much larger than the tunnel drainage. And the applicability of conventional mountain tunnel waterproofing and drainage systems in water-rich karst tunnels was investigated. According to the effect of water pressure reduction behind the lining, based on the conventional waterproofing and drainage systems, an improvement scheme was proposed. The research results can provide reference for the optimal design of waterproofing and drainage in water-rich karst tunnels.

Water pressure distribution on linings of water-rich karst tunnels with a conventional mountain tunnel drainage scheme

Conventional waterproofing and drainage schemes for mountain tunnels

For mountain tunnels without special requirements of environmental protection, tunnel waterproofing and drainage are generally designed according to the general reference drawing (Fang et al. 2016; Yuan et al. 2000), henceforth called the conventional scheme. The conventional waterproofing and drainage system of a mountain tunnel comprises a waterproof board, non-woven fabric, circumferential drainage pipe, longitudinal drainage pipe, transverse connection pipe and central drainage ditch (Fig. 3). The details are as follows:

1. A waterproof layer is laid between the initial support and the secondary lining of the tunnel, which comprises a “geotextile + waterproof board.” In the area of the tunnel crown and wall, a layer of geotextile is laid first, followed by an ethylene–vinyl acetate copolymer smooth waterproof board.
2. On the outer side of the lining of the left and right side walls of the tunnel, at a height of 30 cm above the bottom of the lateral ditch of the tunnel, a longitudinal

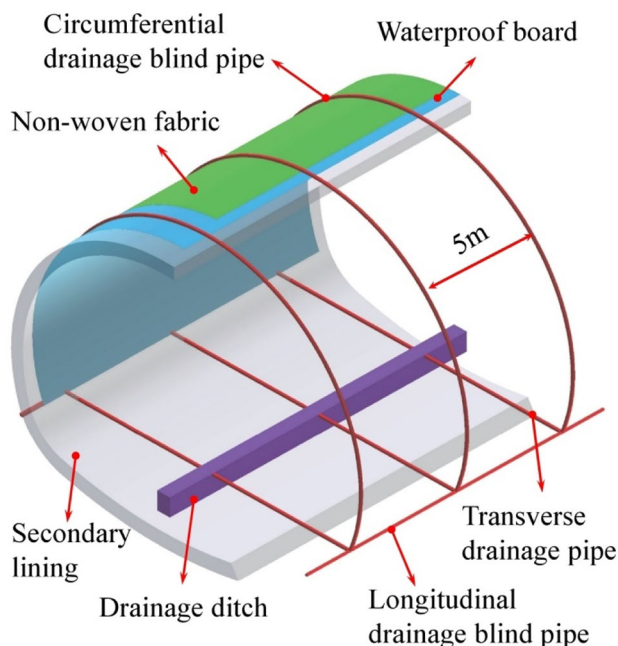


Fig. 3 Conventional waterproofing and drainage system of mountain tunnels

blind pipe with a diameter of 100 mm is set up. The pipe is made of double-walled high-density polyethylene (HDPE) perforated bellows with a diameter of 100 mm and a wall thickness of 4 mm. It is wrapped in non-woven fabric and tied tightly at intervals with hemp rope or pervious cloth tape, with a spacing of no more than 20 cm.

3. In the tunnel lining crown and side wall region, a circular blind pipe with a diameter of 100 mm is set. The pipe is made of HDPE with small holes, and the thickness is 3 mm, wrapped in non-woven fabric. The circular blind pipes are tied in the same way as the longitudinal blind pipe with a longitudinal spacing of 5 m.
4. The tunnel lateral drainage ditch is connected by transverse water conduits which are made of polyvinyl chloride pipes with a diameter of 100 mm.

For general mountain tunnels, the tunnel lining does not bear water pressure. Groundwater in the surrounding rock around the tunnel is concentrated in the central drain of the tunnel through the circumferential drain blind pipe and the longitudinal drain blind pipe behind the lining, and is finally discharged outside the tunnel (Hwang and Lu 2007; Li et al. 2009). For tunnels in non-karst areas, the permeability coefficient of the surrounding rock is small, the effect of surface rainfall on the tunnel is smaller, and the groundwater volume around the tunnel is also small. All groundwater flowing to the tunnels can be discharged (Wang et al. 2008). Therefore, the conventional waterproofing and drainage methods can meet the requirements of tunnel drainage and tunnel lining does not bear water pressure. However, for water-rich karst tunnels, the permeability coefficient of the surrounding rock is relatively large and the groundwater in the rock surrounding the tunnel is recharged by surface rainfall. The cases presented in Fig. 2 have also shown that the conventional waterproofing and drainage system needs further improvement in water-rich karst tunnels.

Water pressure distribution on the lining of water-rich karst tunnels

Numerical model and boundary conditions

Three-dimensional numerical models of shallow and deep tunnels were established using the New experience of Geo-Technical analysis System (MIDAS GTS/NX), developed by MIDAS IT. The overburden of the shallow and deep tunnels is 12 and 49.7 m, respectively. The size of shallow tunnel model is: $L \times W \times H = 115 \text{ m} \times 14 \text{ m} \times 74 \text{ m}$, and the size of deep tunnel model is: $L \times W \times H = 115 \text{ m} \times 14 \text{ m} \times 112 \text{ m}$, the distance between the lower boundary and the bottom of the tunnel is 49.7 m. The surrounding rock, waterproof board, non-woven fabric, drainage pipe, and central drainage ditch

are all simulated by solid elements. The Mohr–Coulomb constitutive model is used for the surrounding rock, and the elastic constitutive model is used for the lining, drainage pipe, waterproof board, and non-woven fabric (Akbarian et al. 2018; Chau and Jiang 2002). The mesh of the numerical models is shown in Fig. 4.

There are five model seepage boundary conditions. First, the top surface of the model is a horizontal plane, and the initial water head does not decrease with the drainage of the tunnel (the supply is much larger than the tunnel drainage capacity). Second, the initial water head height on the lining crown of the shallow tunnel is 12 m, and that of the deep tunnel is 50 m. Third, the left and right sides of the model and the front and rear boundaries are stable boundaries, and the water heads of each point are equal, namely, $H=h$. Fourth, the bottom of the model is an impervious boundary, and the normal velocity and flow rate are both 0. Fifth, the water head of the central drainage ditch section at $Y=0$ m and $Y=14$ m is set to 0.

Calculation parameters

Class C25 shotcrete is used for the primary support of the tunnel and class C35 moulded reinforced concrete is used for the secondary lining of the tunnel. The thicknesses of the

waterproof board and non-woven fabric are 3 mm each, the diameter of the drainage blind pipe is 10 cm and the size of the central drainage ditch is length \times width = 84.4 cm \times 60 cm. The parameters of various materials are selected according to previous studies (Ma et al. 2016; Hu et al. 2019), as shown in Table 1.

Water pressure distribution

Under the stable drainage conditions of the tunnel, the distribution of pore water pressure in the surrounding rock along the buried depth of the tunnel is shown in Fig. 5.

It can be seen from Fig. 5a that when the conventional waterproofing and drainage system is used in shallow water-rich karst tunnels, the pore water pressure in the tunnel surrounding rock is almost unchanged along the direction of tunnel depth, owing to the shallow burial depth. When the depth of the tunnel increases, the rate of reduction in water pressure in the stratum increases gradually and the water pressure acting on the tunnel lining also decreases to a certain extent, as shown in Fig. 5b. It also can be seen from Fig. 5 that the water pressure at the foot of the side wall is reduced significantly. It revealed that the water pressure around the lining can be greatly reduced by setting drainage blind pipes.

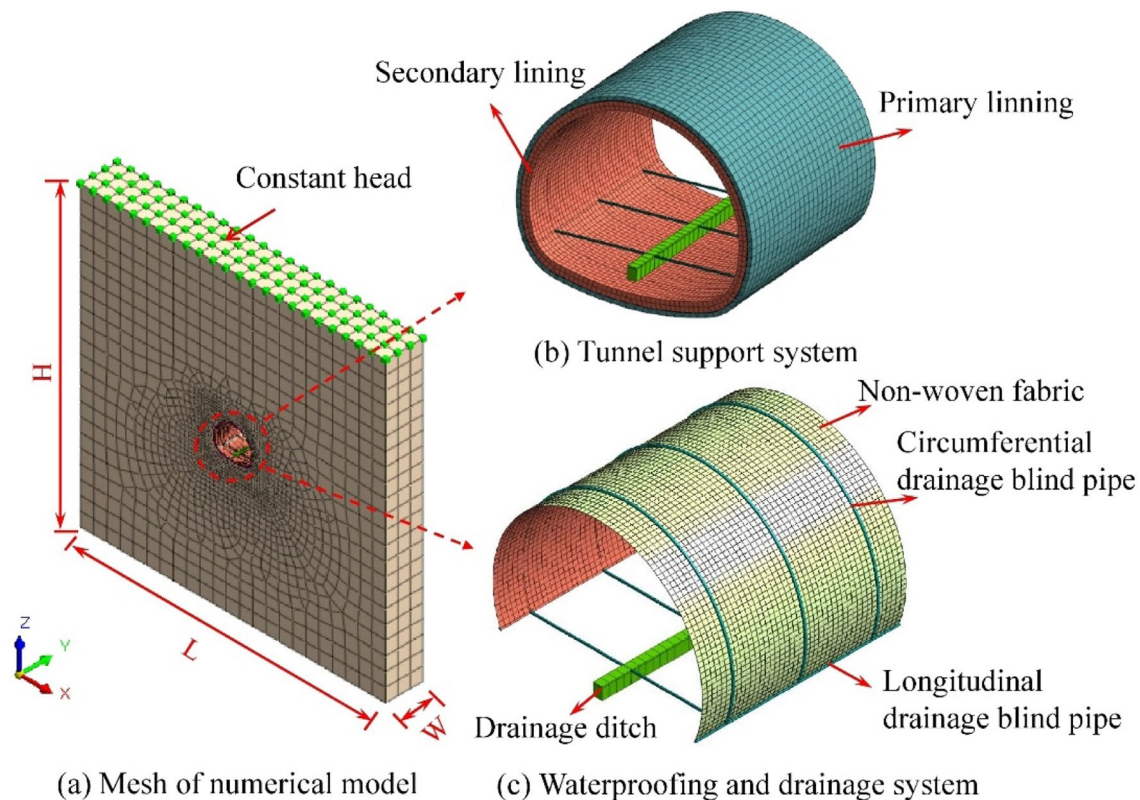


Fig. 4 Mesh of numerical model. **a** Mesh of numerical model; **b** tunnel support system; **c** waterproofing and drainage system

Table 1 Calculation parameters of various materials

Materials	Elastic Modulus /Gpa	Bulk density /kN/m ³	Poisson's ratio	Cohesion /MPa	Internal friction angle/°	Permeability coefficient /m/s
Surrounding rock of tunnel	1.8	21.5	0.3	0.45	55	2e−6
Primary support	23	22	0.20	–	–	2e−8
Secondary lining	32.5	25	0.20	–	–	2e−10
Circumferential drainage blind pipe	0.65	9.32	0.20	–	–	4e−2
Central drainage ditch	21	22	0.20	–	–	4e−2
Waterproof board	0.065	9.8	0.25	–	–	4e−11
Non-woven fabric	0.065	6	0.25	–	–	8e−6

To analyse the distribution of water pressure behind the tunnel lining along the horizontal and vertical directions, water pressure observation lines were arranged along the longitudinal direction of the tunnel in the tunnel crown, waist, side wall, side wall foot and invert centre; and a typical cross section was selected at $Y=9.5$ m in the middle of the model (to eliminate the boundary effect). The results of water pressure distribution along the longitudinal and transverse directions of the shallow and deep tunnel lining are shown in Figs. 6 and 7, respectively.

It can be seen from Fig. 6 that, for the shallow tunnel, the water pressure on the tunnel lining is close to the hydrostatic pressure and the water pressure at the foot of the invert and the side wall is reduced. The water pressure along the longitudinal direction of the tunnel lining varies a little, the water pressure at the circumferential drainage blind pipe (2, 7 and 12 m) is reduced slightly, whereas the water pressure at the centre of the invert is reduced significantly. The results of the water pressure for a typical cross section of the tunnel ($Y=9.5$ m) show that the water pressure of the crown was 112 kPa when the water head on the top of tunnel is 12 m, which is 5.1% less than the static water pressure of 118 kPa. The water pressure at the foot of the side wall was 80 kPa, which is reduced by 62.6% compared with the static water pressure of 214 kPa. It is related to the existence of longitudinal drainage pipes in this section. The water pressure in the centre of the invert was 174 kPa, which is 26.3% lower than the hydrostatic pressure 236 kPa.

Figure 7 presents that, the distribution of water pressure behind the lining in the deep tunnel is markedly different from that of the shallow tunnel. For the deep karst tunnel, the water pressure at the crown and wall changes markedly along the longitudinal direction. The water pressure at the section of the circular drainage pipe (2, 7 and 12 m) tends to zero, whereas the water pressure at the middle of the two circular drainage pipes reaches its peak. Owing to the drainage effect of the longitudinal drainage blind pipe, the water pressure along the foot of the longitudinal side wall of the tunnel maintained a low value (about 30 kPa), whereas the

invert centre maintained a high water pressure because of the lack of a drainage system. The water pressure of the crown was 302 kPa, which is 38.4% less than the hydrostatic pressure (490 kPa). The water pressure at the centre of the invert was 481 kPa, which is reduced by 21.0% compared with the hydrostatic pressure (609 kPa). The above results show that when the conventional waterproofing and drainage scheme is applied to the water-rich karst tunnel, in the case of a large amount of rainfall replenishment, the tunnel's drainage system cannot discharge the groundwater in time. And then, high water pressure will be generated at the invert which will cause safety hazards for the tunnel structure.

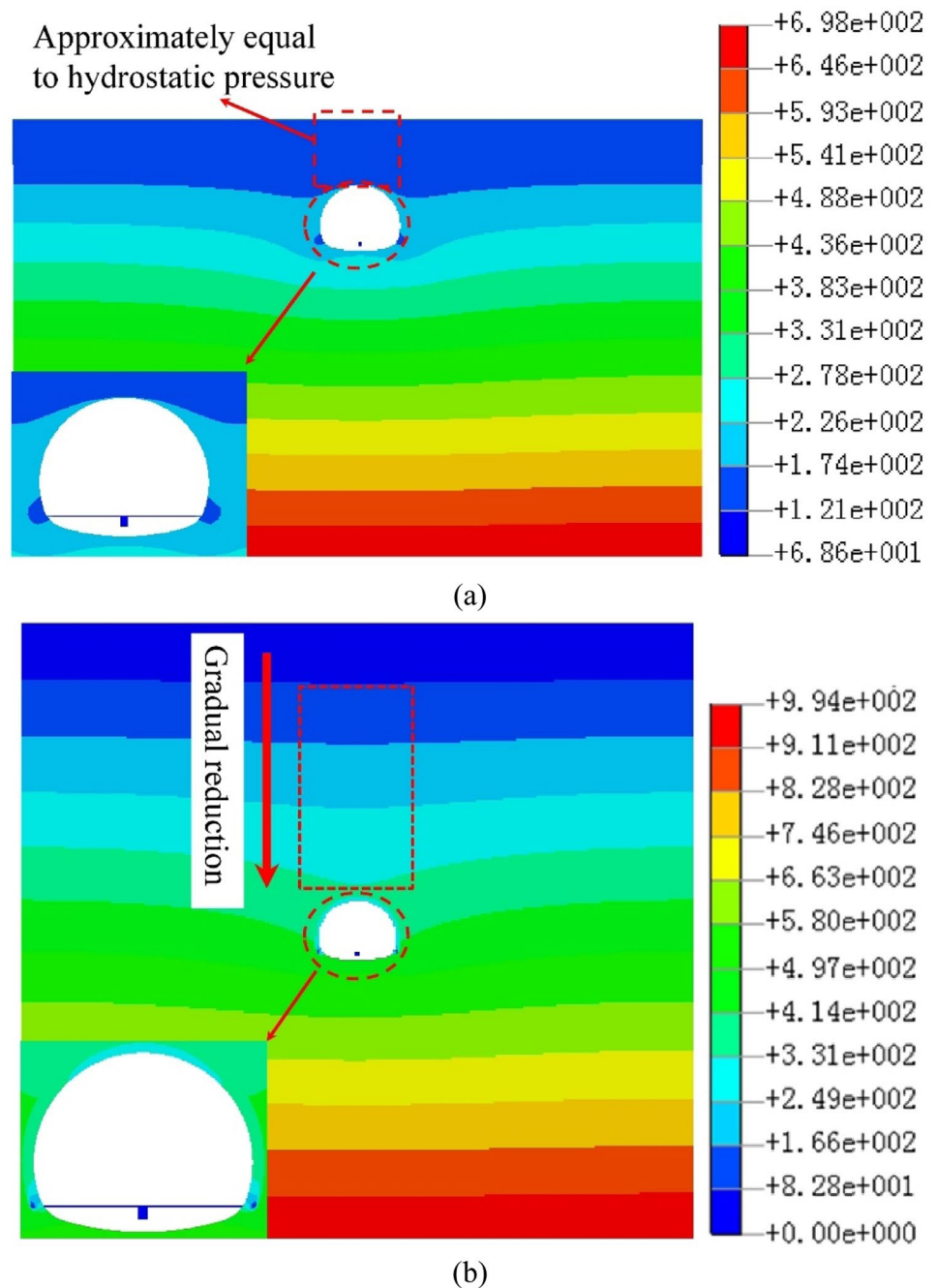
In the case of the water-rich shallow tunnel, owing to the small depth of the tunnel, the water pressure will not affect the safety of the tunnel structure. As for the water-rich deep karst tunnel, the drainage system has a better water pressure reduction effect at the crown and wall of the tunnel lining, but there is almost no reduction at the invert. The tunnel invert is the weak part of the structure; under the action of water pressure, invert uplift, cracking and other disorders easily appear during operation (see Fig. 2 for examples). Therefore, it is necessary to optimise the waterproofing and drainage schemes for water-rich karst tunnels, so that their structure can withstand higher water pressure and reduce structural damage caused by water.

Optimisation of waterproofing and drainage for water-rich karst tunnels

Optimised drainage scheme for karst tunnels

When optimising the waterproofing and drainage system of tunnels, to facilitate design and construction, major changes in conventional schemes should be avoided. The analysis in Sect. 2.2 demonstrated that the reduction rate of water pressure at the invert area was very small, when the conventional waterproofing and drainage scheme was adopted, as there was no drainage pipe at the centre of the tunnel invert, the

Fig. 5 Law of pore water pressure distribution along the depth direction. **a** The shallow tunnel; **b** the deep tunnel



structure has a low resistance to water pressure. Therefore, the optimisation scheme should aim at effectively reducing the water pressure of the invert. Based on this consideration, three waterproofing and drainage optimisation schemes were proposed, labelled optimised scheme A, B and C.

Optimised scheme A: circular drainage blind pipes of the lining crown and wall are encrypted (Fig. 8a). The main purpose of this scheme is to increase the overall drainage capacity of the tunnel by encrypting the circumferential drainage blind pipe, so as to reduce the water pressure of the tunnel invert. In this study, three cases

of reducing the spacing of circumferential drainage pipes from 5 to 4, 3 and 2 m were analysed.

Optimised scheme B: a longitudinal drainage blind pipe with the same diameter as the circumferential drainage blind pipe is added to the bottom of the tunnel. At the same time, the circumferential drainage blind pipe is extended to the bottom of the invert to connect with the longitudinal drainage blind pipe. The longitudinal drainage blind pipe at the bottom of the invert is connected with the central drainage ditch through the vertical drainage blind pipe (Fig. 8b). The purpose of the scheme is to

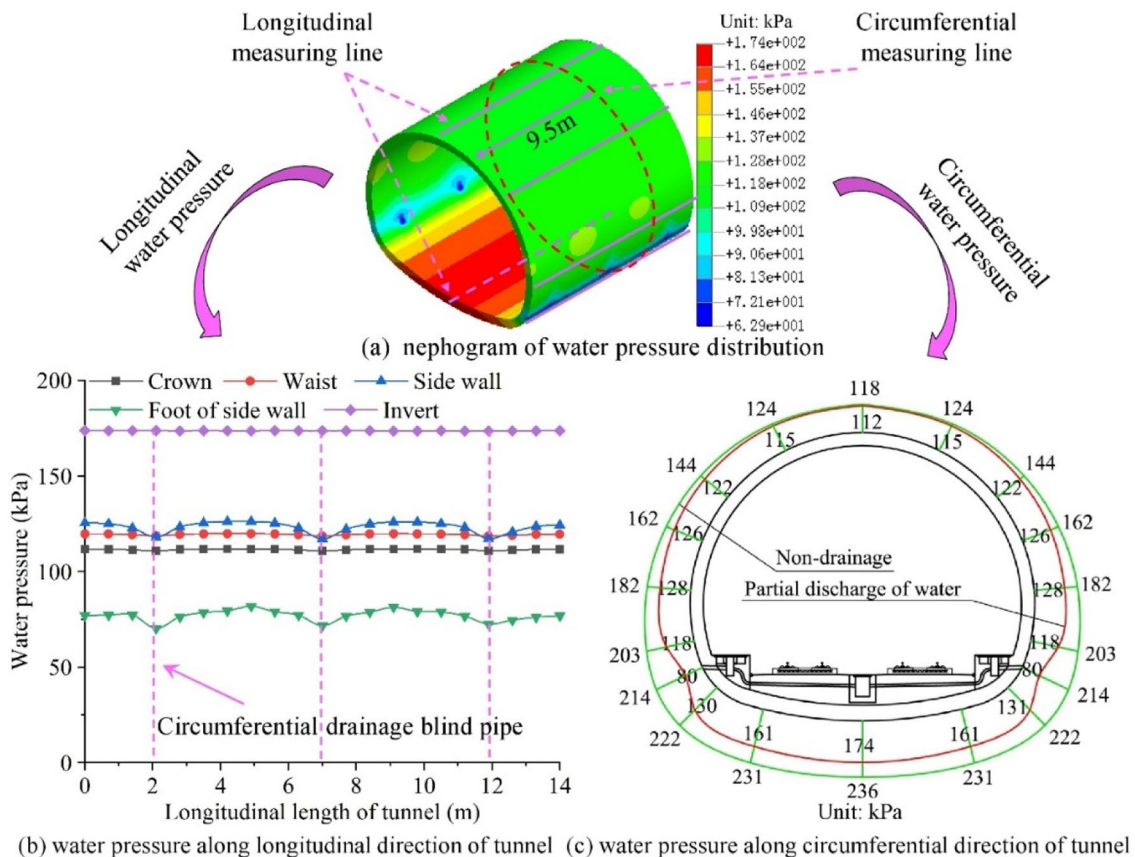


Fig. 6 Law of water pressure distribution at the lining of shallow karst tunnel. **a** Nephogram of water pressure distribution; **b** water pressure along longitudinal direction of tunnel; **c** water pressure along circumferential direction of tunnel

reduce the water pressure of the invert by improving the drainage capacity of the invert area.

Optimised scheme C: the central drainage ditch of the tunnel is moved from the inside of the invert to its outside. Meanwhile, the circumferential drainage blind pipe is extended to the central drainage ditch (Fig. 8c). Schemes C and B both reduce the water pressure of the invert by increasing the drainage capacity of the invert area; however, the drainage path of karst water is different. The karst water at the bottom of the invert in scheme B should flow upward into the drainage ditch through the vertical connecting pipe. However, the karst water at the bottom of the invert in scheme C can be drained down into the drainage ditch, which is more conducive to the drainage of the tunnel karst water.

Water pressure distribution in the optimized schemes

Numerical models and calculation parameters

Three-dimensional numerical models were established to simulate the optimised schemes. The calculation

models were improved based on the model of the deep tunnel described in Fig. 4. The conventional half-pack and half-drain schemes were replaced by the schemes shown in Fig. 8. The water pressure distribution on the lining under different schemes was analysed and compared with that of the conventional scheme. The boundary conditions and calculation parameters of the model were same as in Fig. 4 and Table 1.

Water pressure distribution behind the lining

For the optimised scheme A, the water pressure distribution of the lining under different spacing of the circumferential drainage blind pipes was similar. Here, taking the circumferential drainage blind pipe spacing of 3 m as an example, the water pressure distribution behind the lining along the longitudinal and transverse direction of the tunnel was analysed. The water pressure distribution behind the tunnel lining under drainage conditions, when the water head of the tunnel crown was 50 m, is shown in Fig. 9. The water pressure distribution on the lining relative to changes in the spacing of the circumferential drainage pipes is shown in Fig. 10.

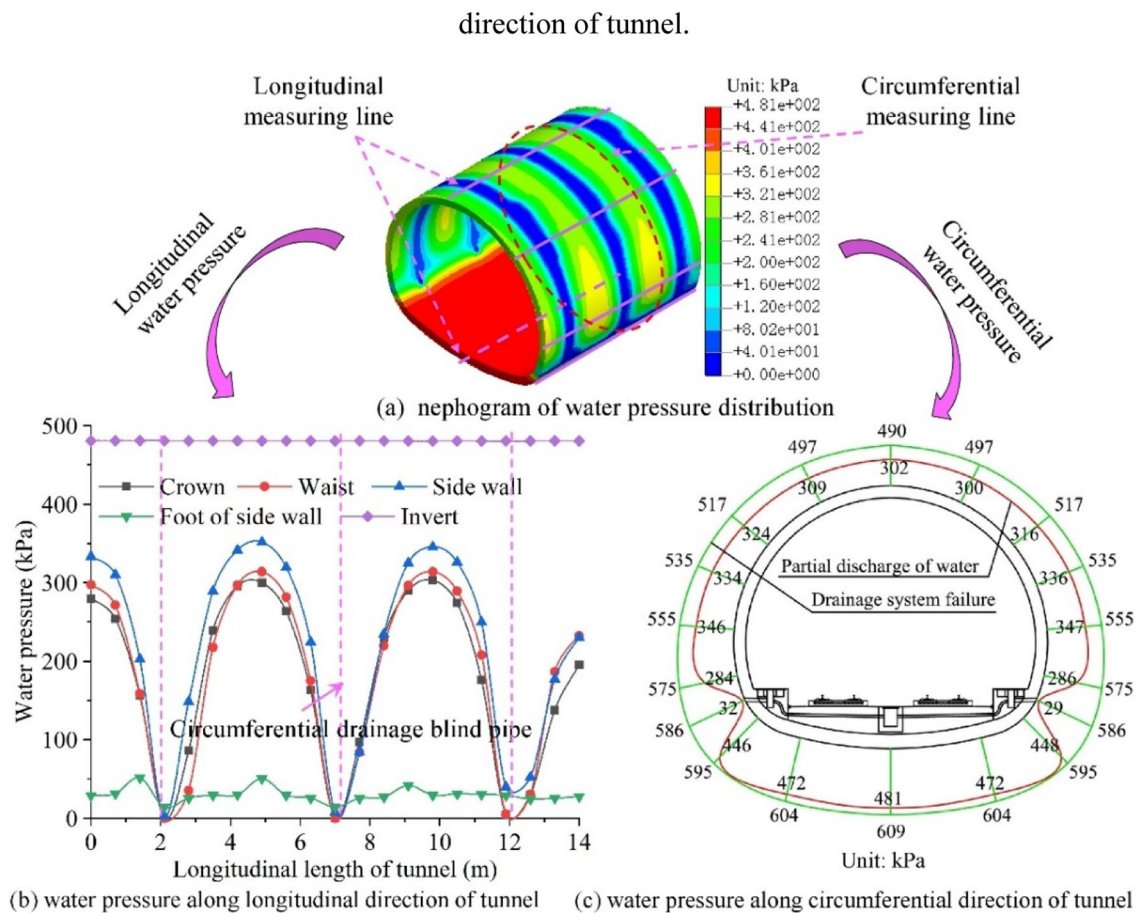


Fig. 7 Law of water pressure distribution at the lining of deep karst tunnel. **a** Nephogram of water pressure distribution; **b** water pressure along longitudinal direction of tunnel; **c** water pressure along circumferential direction of tunnel

As can be seen from Fig. 9, the water pressure distribution in the tunnel cross section when the circumferential drainage blind pipe is encrypted was basically the same as that in the non-encrypted condition. The water pressure was close to 0 at the locations of the circumferential and longitudinal drainage blind pipes and the water pressure was higher at the bottom of the invert. After the circumferential drainage pipe was encrypted, the water pressure at the crown of the tunnel decreased significantly; however, it decreased only slightly at the invert. When the water head was 50 m above the tunnel crown, the water pressure of the crown was 165 kPa, which is 66.3% less than the hydrostatic pressure (490 kPa). The water pressure at the centre of invert was 458 kPa, which is 24.8% less than the hydrostatic pressure (609 kPa). Comparing with Fig. 7, it can be seen that when the circumferential drainage pipe was encrypted (from 5 to 3 m), the water pressure at the crown area decreased considerably. However, the decrease in water pressure at the invert area was not clear, increasing only from 21.0 to 24.8%.

It can be seen from Fig. 10 that the water pressure at each part of the tunnel decreased approximately linearly,

when the spacing of the circumferential drainage blind pipes was gradually reduced from 5 to 2 m. The rate of decrease in water pressure at the crown area was higher than that at the invert area. Furthermore, the invert area always bore a large water pressure. It was found that the optimised scheme A could improve the drainage capacity of the arch area of the lining, but the effect was limited in the invert area, as the invert has weak water pressure resistance because of its small curvature and it easily fails under high water pressure.

For optimised schemes B and C, the distribution of water pressure behind the tunnel lining are shown in Figs. 11 and 12, respectively, when the total water head at the crown of the tunnel was 50 m.

It can be seen from Fig. 11 that the reduction in water pressure under the tunnel invert decreased markedly when the optimised scheme B was adopted for drainage. The rate of decrease in water pressure of the invert increased considerably, because of the influence of the circumferential and longitudinal drainage blind pipes at the bottom of the invert. When the water head was 50 m above the tunnel crown, the water pressure at the tunnel crown was 233 kPa, which

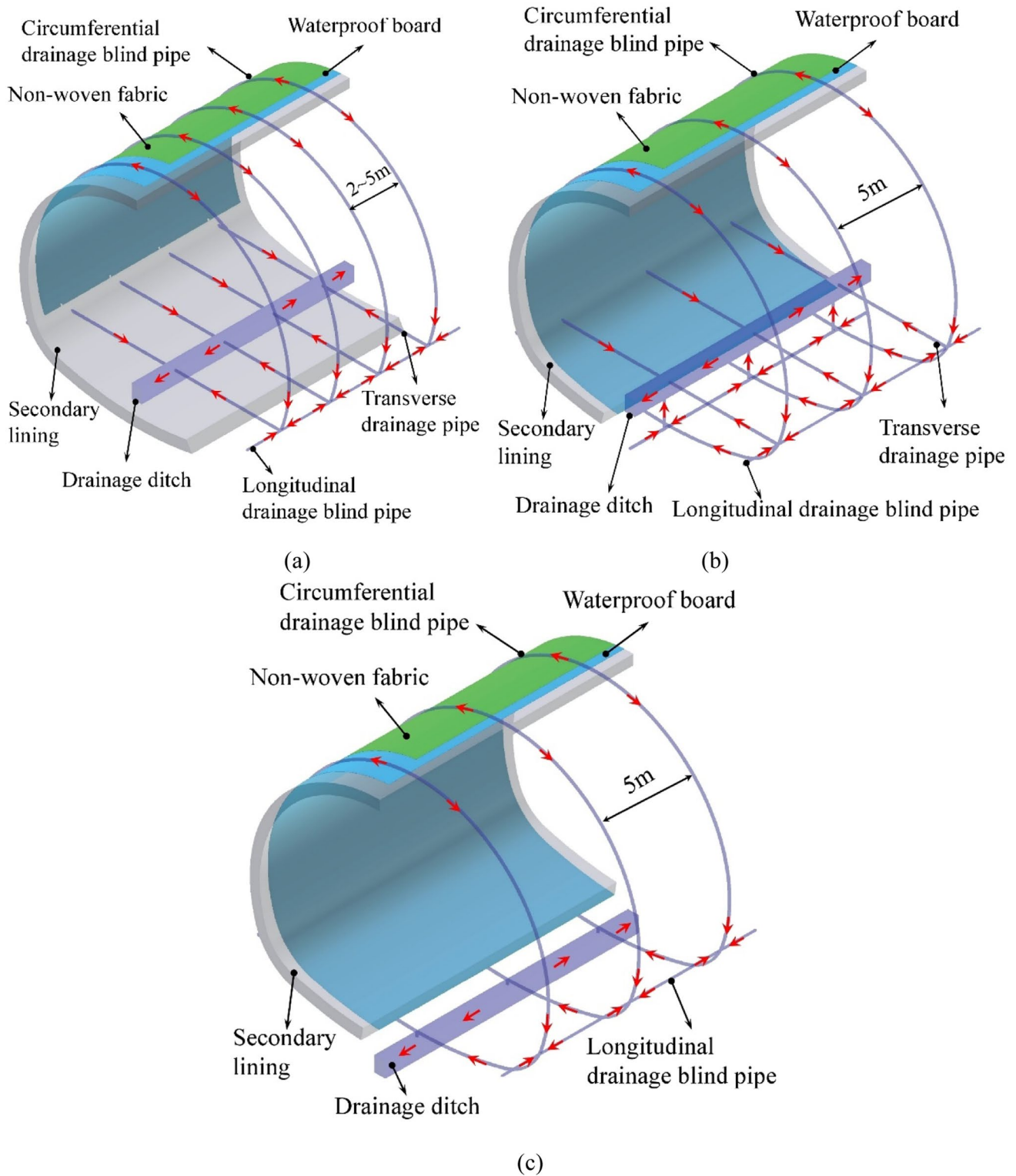


Fig. 8 Optimization schemes of tunnel waterproof and drainage. **a** Optimised scheme A; **b** optimised scheme B; **c** optimised scheme C

is 52.5% less than the hydrostatic pressure (490 kPa); the water pressure at the centre of the invert was 100 kPa, which is 83.6% less than the hydrostatic pressure (609 kPa). The

reduction in water pressure in scheme B was more significant compared with that in conventional schemes.

As can be seen from Fig. 12, the reduction in water pressure under the invert was very large, when the

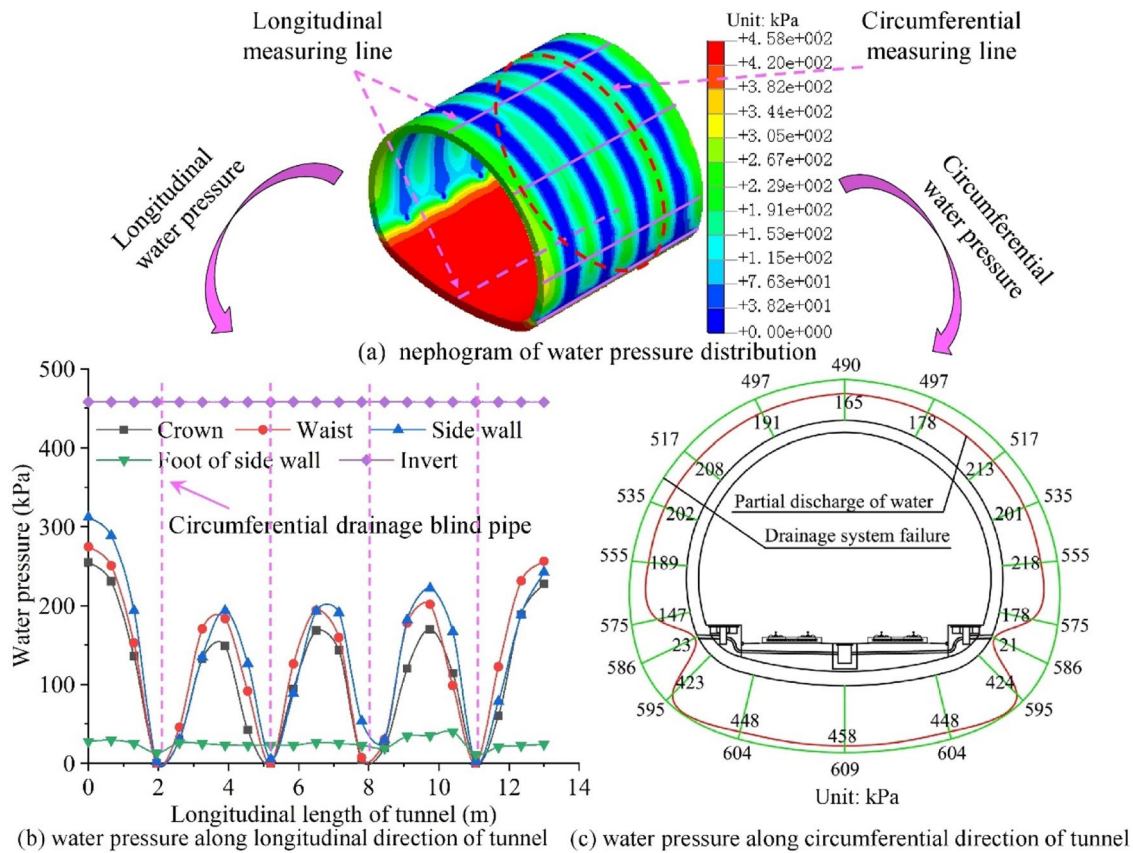
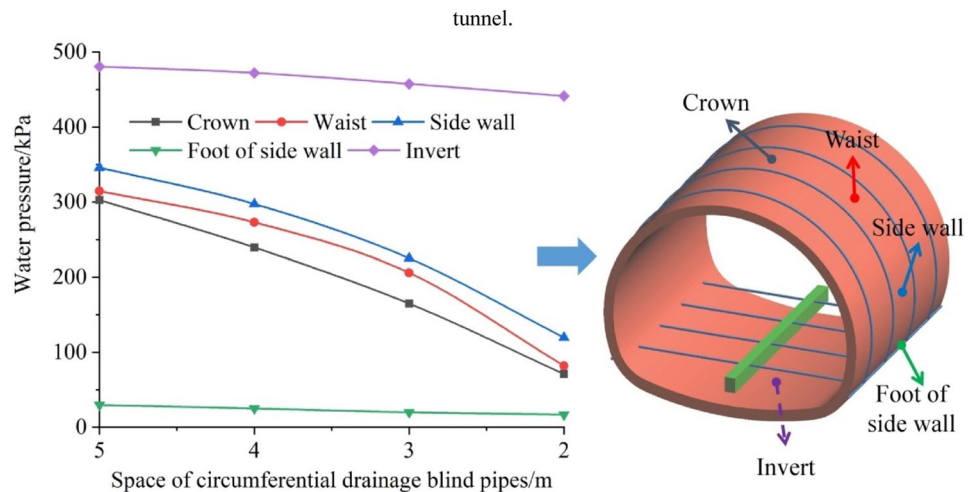


Fig. 9 Law of water pressure distribution in optimised scheme A. **a** Nephogram of water pressure distribution; **b** water pressure along longitudinal direction of tunnel; **c** water pressure along circumferential direction of tunnel

Fig. 10 Relationship between the distance between circular drainage blind pipes and the water pressure behind the lining in scheme A



optimised scheme C was adopted. The water pressure at the tunnel crown decreased from 490 to 172 kPa (a decrease of 64.9%), when the water head was 50 m above the tunnel crown. The water pressure at the centre of the invert decreased from 609 to 22 kPa (96.4%). This result

demonstrated that the elevation of the drainage point was reduced when the drainage ditch was set at the bottom of the invert. Under the action of gravity, karst water tended to converge downward to the drainage ditch and the reduction in water pressure at the invert was very significant.

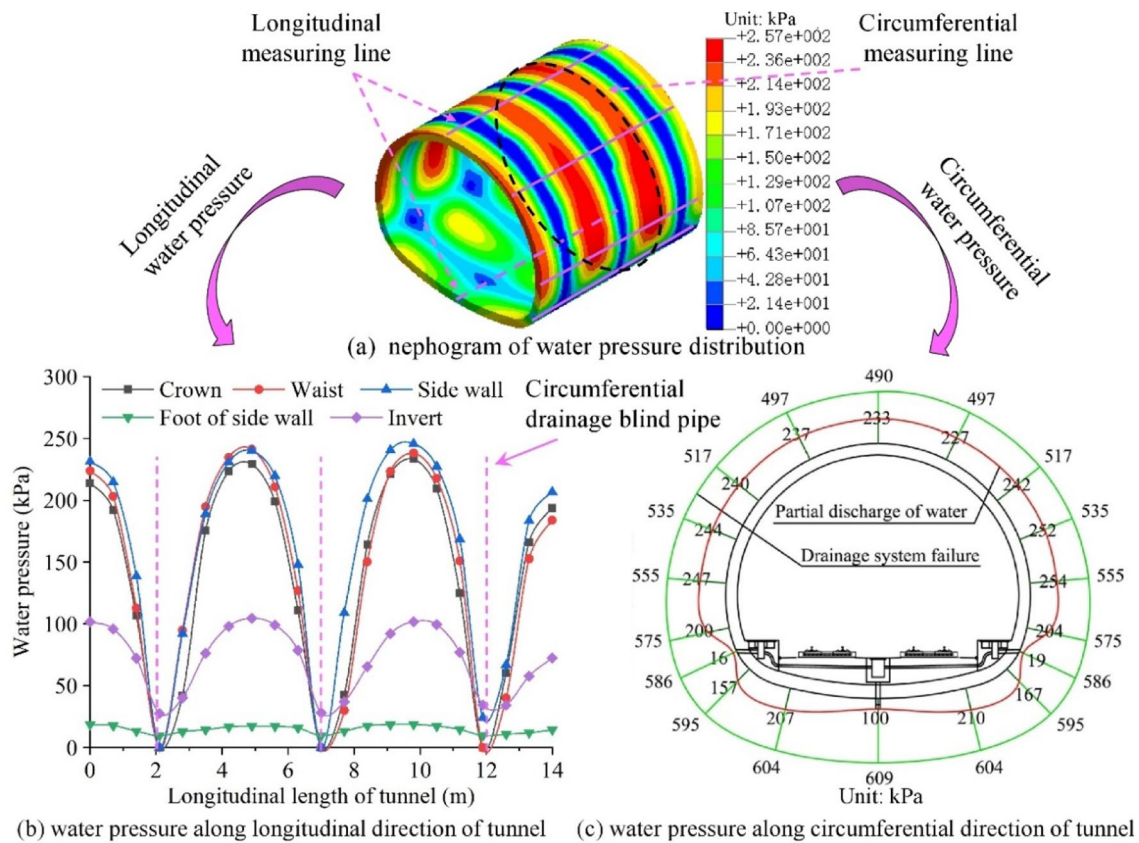


Fig. 11 Law of water pressure distribution in optimised scheme B. **a** Nephogram of water pressure distribution; **b** water pressure along longitudinal direction of tunnel; **c** water pressure along circumferential direction of tunnel

Analysis of different waterproofing and drainage schemes

To analyse the advantages and disadvantages of different waterproofing and drainage schemes, the rate of reduction in water pressure at the tunnel lining crown and the invert, the convenience and durability of waterproofing and smoothness of drainage pipe during operation were investigated for the different proposed schemes and the optimal one was put identified. The comparison results of different waterproofing and drainage schemes are shown in Table 2.

The reduction effect of water pressure behind the lining

When the conventional waterproofing and drainage scheme was adopted, the tunnel lining vault and the invert arch would accumulate large water pressure in the case of sudden rainstorm. When optimised scheme A was adopted, the water pressure of the crown can be greatly reduced, but the invert area still bears large water pressure and the optimisation effect is poor. When the optimised schemes B and C are adopted, the water pressure at the crown and invert area of the tunnel can be greatly reduced and the waterproof and

drainage capacity of the karst tunnel can be significantly improved.

The convenience of construction

The waterproofing and drainage system of optimised schemes A and B was more complex, and there were many connection joints of drainage pipes. The construction process was also complicated, and the drainage pipe was easily damaged. However, optimisation scheme C had fewer construction procedures and the construction quality could be easily guaranteed.

The smoothness of drainage pipe during operation

When optimised scheme B was adopted, the karst water in the invert area needed to flow upward from the vertical connecting pipe into the central drainage ditch. This was not conducive to drainage and the drainage pipe was easily blocked during long-term operation. In optimised scheme C, the central drainage ditch was set at the bottom of the invert to reduce the elevation of the drainage point. It was more

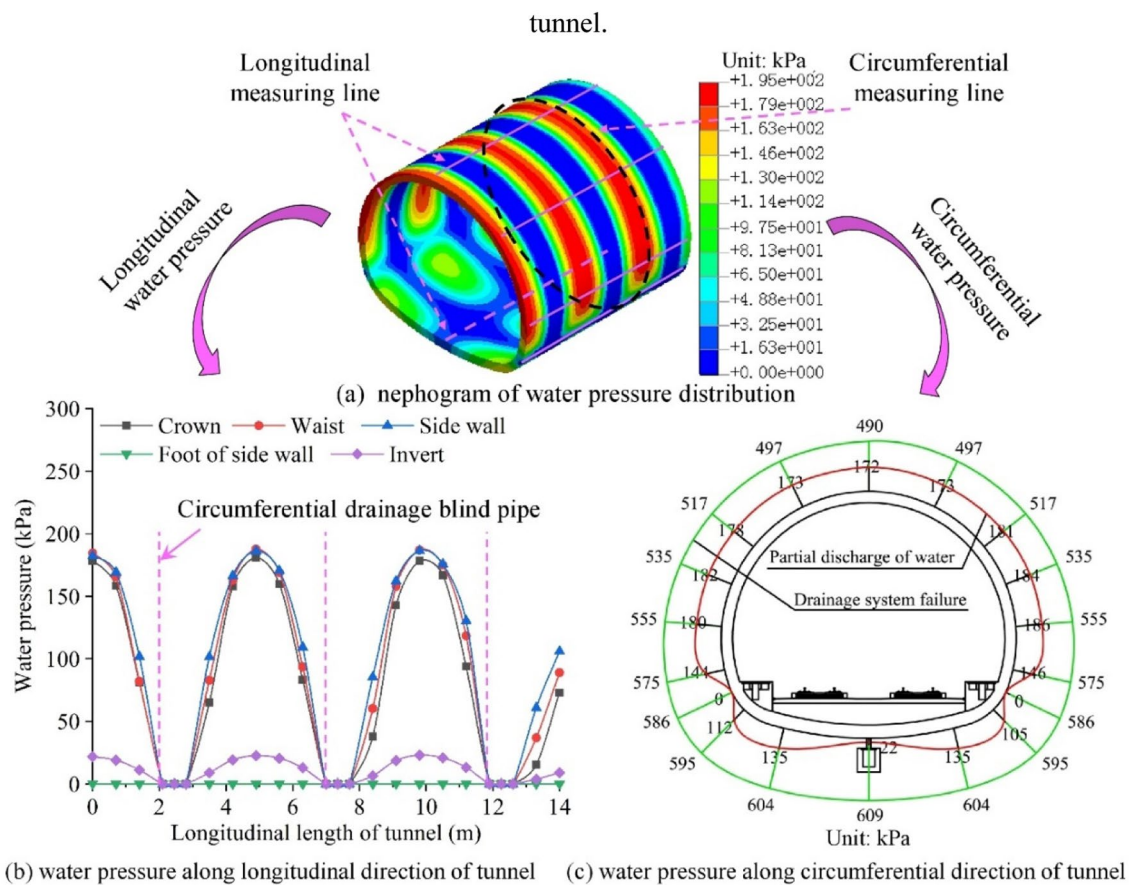


Fig. 12 Law of water pressure distribution in optimised scheme C. **a** Nephogram of water pressure distribution; **b** water pressure along longitudinal direction of tunnel; **c** water pressure along circumferential direction of tunnel

Table 2 Comparison of different waterproofing and drainage schemes

Schemes	Water pressure at crown (kPa)			Water pressure at invert (kPa)			Convenience	Smoothness
	Hydrostatic Pressure	Drainage	Reduction rate (%)	Hydrostatic Pressure	Drainage	Reduction rate (%)		
Conventional scheme	490	302	38.4	609	481	21.0	Common	Common
Scheme A	490	165	66.3	609	458	24.8	Complex	Common
Scheme B	490	233	52.4	609	100	83.6	More complex	Poor
Scheme C	490	172	64.9	609	22	96.4	Simple	Better

conductive to the discharge of water and drainage pipe is not easy to be blocked during operation.

From the above analysis, it can be seen that the optimised scheme C could reduce the water pressure at the crown and invert of the tunnel substantially. The waterproofing and drainage capacity of the karst tunnel and the safety reserve of the lining structure were also improved considerably, and the scheme was easy to construct. Moreover, only minor changes to the conventional scheme are required. Therefore, for water-rich karst tunnels with abundant rainfall, it is

suggested that drainage ditches should be set at the bottom of the tunnels.

Model test of waterproofing and drainage optimisation for water-rich karst tunnels

To test the waterproofing and drainage effect of optimised scheme C, model tests similar to those conducted for water pressure were performed for karst tunnel drainage. The

distribution of water pressure on the lining was analysed when the drainage ditch was set at the bottom of the invert.

Test platform and similarity relation

To carry out the experimental study on waterproofing and drainage of water-rich karst tunnels, a special water pressure test platform for karst tunnels was developed, as shown in Fig. 13. The size of the box was 1.00 m × 2.25 m × 2.25 m. The geometry and volume-weight similarity ratios were 20:1 and 2:1, respectively, i.e., $c_L=20$ and $c_\gamma=2$. Based on the three basic theorems of similarity theory and the results of similar model tests (Lei et al. 2015, 2016; Ye et al. 2014), the other similarity parameters can be determined. The similarity parameters of the model test are shown in Table 3.

Similarity materials and test model

The fine sand and quartz sand was used to simulate the surrounding rock of the tunnel. The permeability coefficient of the surrounding rock was 2×10^{-6} m/s (Xiao et al. 2018) and the ratio of quartz sand to fine sand was 1:3. The secondary lining was simulated by 2.5 cm of gypsum, according to geometrical similarity (Lei et al. 2015). The strength and ratio of gypsum were determined by strength similarity. The ratio of gypsum to water was 1:3, after comparing several groups of tests. Waterproof board and circumferential drainage blind

Table 3 Similarity parameters of the model test

Physical indexes	Similarity relation	Similarity ratio
Geometry L	$C_L=20$	20
Volume-weight γ	$C_\gamma=2$	2
Elastic modulus E	$C_E=C_L C_\gamma$	40
Poison's ratio μ	$C_\mu=1$	1
Stress σ	$C_\sigma=C_L C_\gamma$	40
Strain ϵ	$C_\epsilon=1$	1

pipe were wrapped on the outside of the tunnel lining. The different drainage conditions were controlled by the drainage pipe set on the front of the model box; valves 1#, 2# and 3# should be opened in the optimised scheme C. The test model and waterproof and drainage system were shown in Fig. 14.

Layout of monitoring points

High sensitivity static strain gauge UT7110Y, produced by Yutai Electronic Technology Co., Ltd., Wuhan city, China, and strain gauge micro osmometer LY-350, produced by Huacheng Civil Engineering Instrument Factory, Danyang city, China, were used to measure water pressure. The measurement points were laid out in the middle section of the

Fig. 13 Water pressure test platform for the karst tunnel

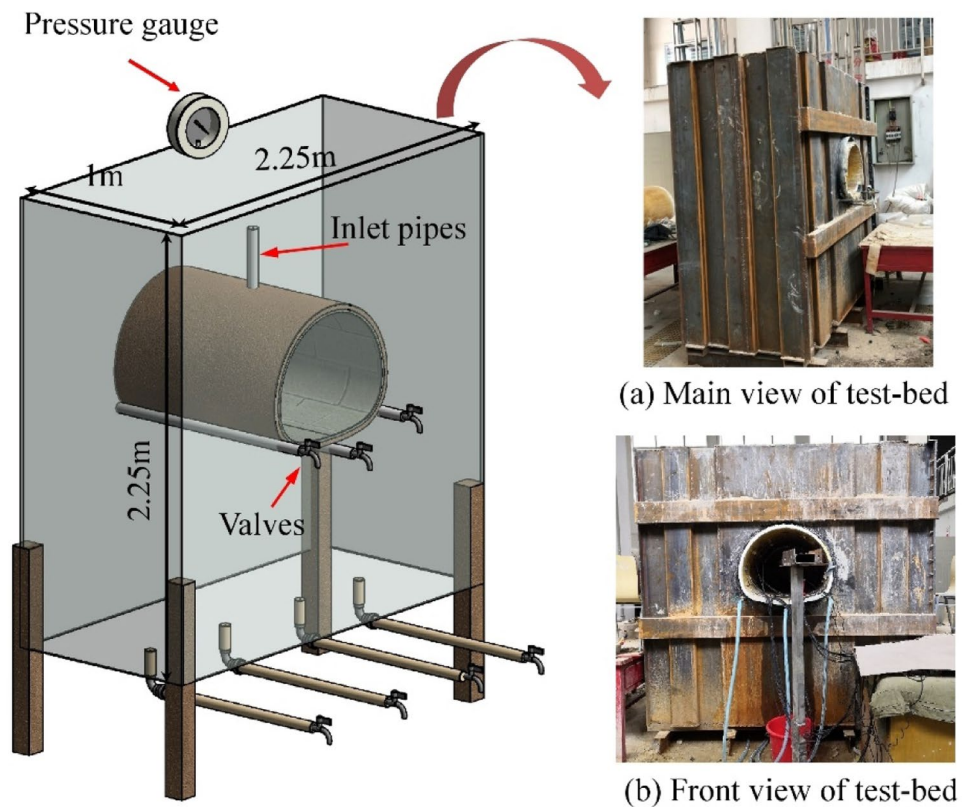
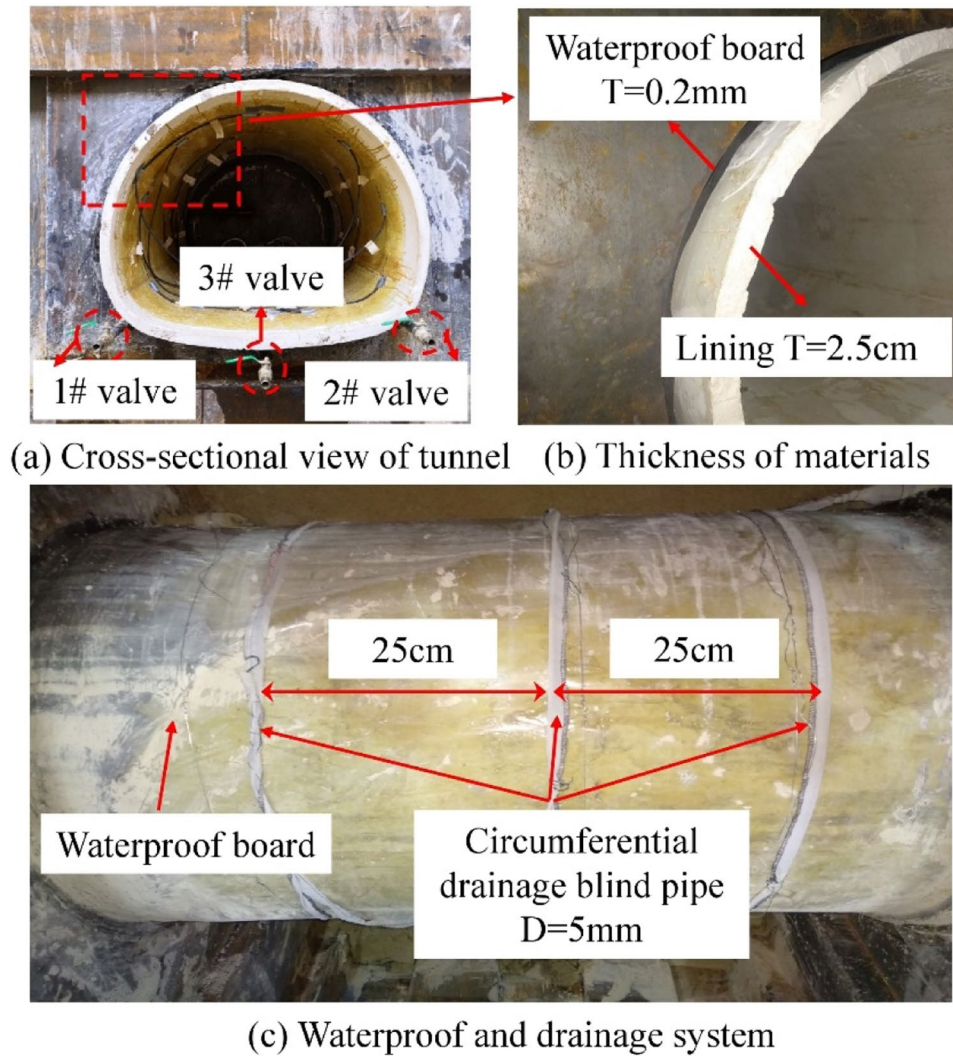


Fig. 14 The test model and waterproof and drainage system. **a** Cross-sectional view of tunnel; **b** thickness of materials; **c** waterproof and drainage system



circumferential drainage pipe and the water pressure monitoring points were set at the crown, waist, side wall, foot of the side wall, middle of the invert and centre of the invert. The layout of water pressure measurement points is shown in Fig. 15.

Water pressure distribution on the tunnel lining

In this test, the maximum water head height at the crown of the lining was 60 cm, which corresponds to the situation when the water head height at the crown is 12 m under practical engineering conditions, considering the bearing capacity of gypsum materials. The distribution of water pressure on the lining with the conventional scheme and the optimised scheme C was tested as shown in Fig. 16; the water pressure in the figures was converted using the similarity relation.

As can be seen from Fig. 16a, the water pressure at each measurement point was equal to the hydrostatic pressure,

when the tunnel was not being drained. For the conventional scheme, the water pressure at the tunnel crown decreased from 116 to 114 kPa (decrease of 1.7%), when the tunnel was drained. The water pressure near the longitudinal drainage pipe decreased from 222 to 34 kPa (decrease of 84.7%) and the water pressure at the tunnel invert decreased from 242 to 190 kPa (decrease of 21.5%). Under the same conditions, the rates of reduction in water pressure at the crown and invert calculated using the numerical method were 5.1% and 26.3%, respectively. The model test results were in good agreement with the numerical results.

As can be seen from Fig. 16b, for the optimised scheme C, the water pressure near the longitudinal drainage blind pipe decreased from 222 to 30 kPa (decrease of 86.5%), when the tunnel was drained. Furthermore, the water pressure at the tunnel invert decreased from 242 to 82 kPa (decrease of 66%). It was shown that the water pressure at the bottom of the invert could be effectively reduced, when the drainage ditch was set at the bottom

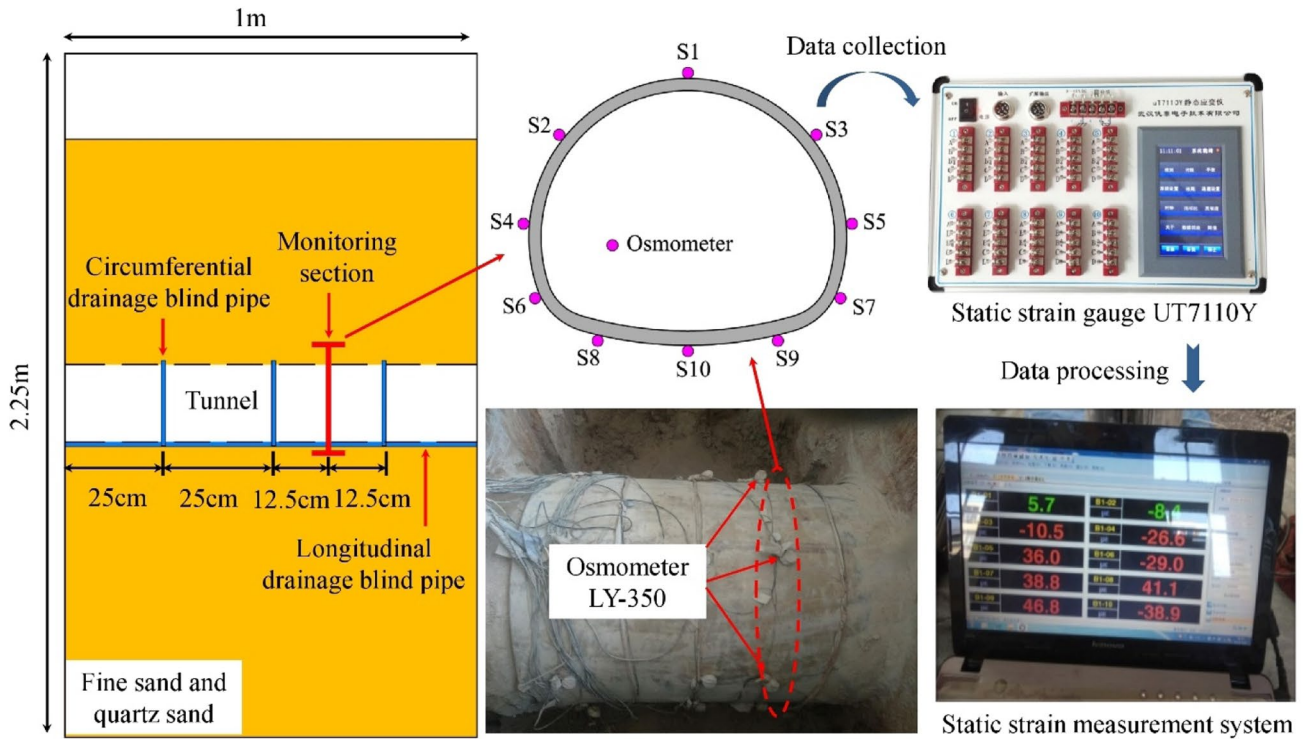
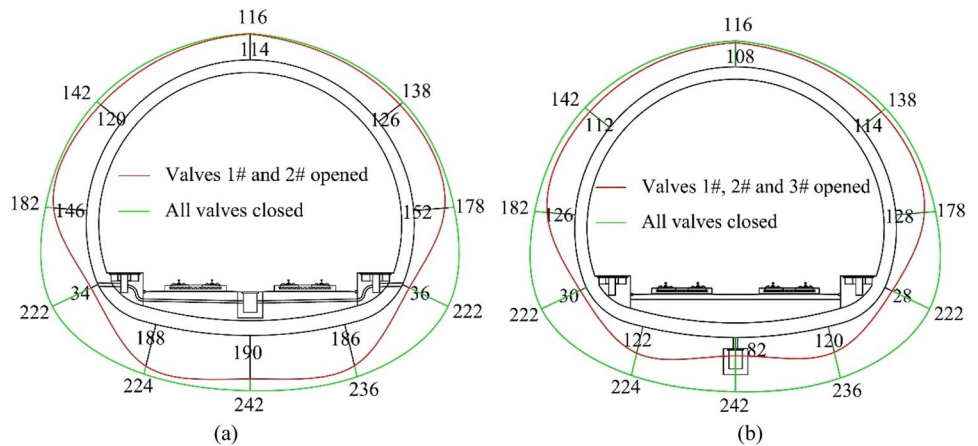


Fig. 15 Layout of water pressure measuring points

Fig. 16 Measured water pressure of model test (kPa). **a** The conventional scheme; **b** the optimised scheme C



of the invert. The overall water pressure bearing capacity of the tunnel structure was also improved. Comparing the results of the numerical simulation in Sect. 3.2, it can be seen that water pressure at the centre of the invert of the tunnel will be reduced greatly, when the optimised scheme C was adopted. Both experimental and numerical simulation results showed that the effect of water pressure reduction is greater when optimised drainage scheme C was adopted.

Discussion

The results of this study presented above show that, when the conventional waterproofing and drainage scheme was applied to the water-rich karst tunnel, the system could not discharge the groundwater in time under a large rainfall supply. High water pressure accumulated in the invert area, threatening the safety of the tunnel structure (as shown

in Figs. 6 and 7). By comparing the advantages and disadvantages of different drainage schemes, it was found that, when the central drainage ditch was placed at the bottom of the invert, the water pressure at the invert area could be greatly reduced and the water pressure resistance of tunnel lining greatly improved. Nam and Bobet (2006) studied the water pressure distribution of lining of water-rich and deep circular tunnel, and also analyzed the scheme of setting the central drainage ditch at the bottom of the tunnel, and their results were in good agreement with those of this paper, as shown in Fig. 17. It could be seen that the optimization scheme C proposed in this paper effectively reduced the water pressure in the invert of the tunnel. The application of this scheme in the water-rich karst tunnel could largely avoid the occurrence of water pressure disease. However, the optimization scheme C proposed in this paper was not suitable for all karst tunnels. In some areas, the development of karst caves were very complex, and there might be large-scale water filled karst caves and underground rivers around the tunnel. The supply of water in this kind of karst caves was usually very large, and it was also obviously supplied by rainfall. It may not be effective to discharge karst water only by optimization scheme C. For this kind of karst caves with large water supply, it was usually necessary to set a water drain hole around the tunnel to ensure the safety of the tunnel.

Following this, numerical simulations and model tests were used to study the distribution of water pressure behind the lining of water-rich karst tunnels. The tunnel lining selected during the study was a common form for grade V surrounding rock and the permeability coefficients of the lining were empirical parameters selected from relevant literature. The changes of lining structure and permeability coefficients impacted the magnitude of the research results.

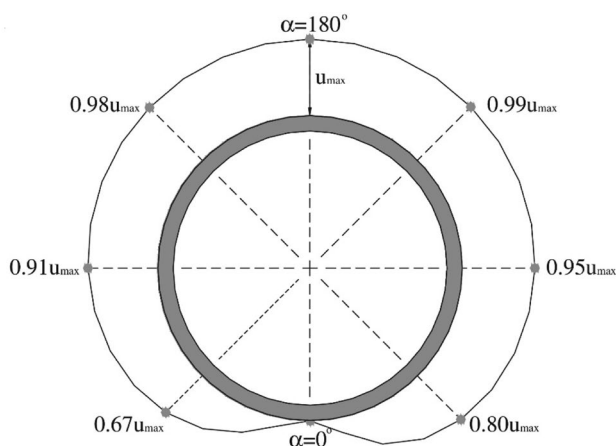


Fig. 17 Pore pressures behind secondary support (Nam and Bobet 2006)

However, the distribution of water pressure behind the lining remained constant.

Further, the karst stratum in this study was equivalent to the homogeneous stratum. The characteristics of water pressure changes caused by pipeline karst were not considered. In view of the complexity of karst strata, Karst passages might be distributed in the crown, waist and side walls of the tunnel, and it might produce local high water pressure around the lining and cause damage to the lining. The water pressure distribution of this situation was also a very complex problem, which would be further studied in the future. In addition, the scale of this model test was 1:20, due to the limitation of the size of the model box, the height from the crown of the tunnel to the top of the model box was 60 cm, which corresponded to 12 m (tunnel depth) of the actual project. This working condition corresponded to the situation of shallow tunnel in the numerical simulation. Therefore, for the conventional waterproofing and drainage scheme, the test results (Fig. 16a) can be compared with the numerical simulation results (Fig. 6c) and the results of the model test were found to be in good agreement with those obtained in the numerical simulation. In future work, it is planned to improve the model scale and model box in a follow-up study and study the effects of optimised scheme C under deep tunnel conditions.

Conclusions

Considering the results obtained in the study, the following conclusions are drawn:

1. When the conventional waterproofing and drainage scheme is adopted and groundwater supply is far greater than the tunnel drainage, the water pressure behind the tunnel lining is in the shape of a “gourd.”
2. For the water-rich karst tunnel with a conventional waterproofing and drainage scheme, the water pressure at the invert of the tunnel lining has a small reduction. And water diseases such as cracking, leakage and invert uplift can easily occur.
3. The water pressure of the lining at the arch area can be effectively reduced by reducing the spacing of the circumferential drainage blind pipes, but the effect of water pressure reduction of lining at the invert area is not clear. Adding a longitudinal drainage blind pipe at the bottom of the invert or placing the central drainage ditch at the bottom of the invert can effectively reduce the water pressure of the lining at the arch and invert area. Therefore, in the case of water-rich karst tunnels, it is recommended to place the central drainage ditch at the bottom of the invert.

Acknowledgements This research is financially funded by Scientific and Technological Innovation Projects with Special Funds for Fundamental Scientific Research Business Fees of Central Universities (No. 2682019CX03), Natural Science Foundation of Hebei Province (No. E2020210068) and State Key laboratory of Mechanical Behavior and System Safety of Traffic Engineering Structures (No. ZZ2020-01).

Compliance with ethical standards

Conflict of interest The authors declare that they have no conflict of interest.

References

- Akbarian E, Najafi B, Jafari M, Faizollahzadeh Ardabili S, Shamsirband S, Chau K (2018) Experimental and computational fluid dynamics-based numerical simulation of using natural gas in a dual-fueled diesel engine. *Eng Appl Comput Fluid Mech* 12(1):517–534
- Casagrande G, Cucchi F, Zini L (2005) Hazard connected to railway tunnel construction in karstic area: applied geomorphological and hydrogeological surveys. *Nat Hazard Earth Sys* 5:243–250
- Chau KW, Jiang YW (2002) Three-dimensional pollutant transport model for the Pearl River Estuary. *Water Res* 36(8):2029–2039
- Fan HB, Zhang YH, He SY, Wang K, Wang XL, Wang H (2018) Hazards and treatment of karst tunneling in Qinling-Daba mountainous area: overview and lessons learnt from Yichang-Wanzhou railway system. *Environ Earth Sci* 77:679
- Fang Y, Guo JN, Grasmick J, Mooney M (2016) The effect of external water pressure on the liner behavior of large cross-section tunnels. *Tunn Undergr Sp Tech* 60:80–95
- Fu G, Cao YP, Zhang L, Zhang CY, Liu HW (2007) The idea of underground water environmental balance applied to the design of the tunnel under high hydrostatic pressures. *Rock Soil Mech* S1:474–478
- Hu J, Wen H, Xie Q, Li B, Mo Q (2019) Effects of seepage and weak interlayer on the failure modes of surrounding rock: model tests and numerical analysis. *Roy Soc Open Sci* 6:190790
- Hwang JH, Lu CC (2007) A semi-analytical method for analyzing the tunnel water inflow. *Tunn Undergr Sp Tech* 22:39–46
- Jeon S, Kim J, Seo Y, Hong C (2004) Effect of a fault and weak plane on the stability of a tunnel in rock: a scaled model test and numerical analysis. *Int J Rock Mech Min Sci* 41:658–663
- Lei MF, Peng LM, Shi CH (2015) Model test to investigate the failure mechanisms and lining stress characteristics of shallow buried tunnels under unsymmetrical loading. *Tunn Undergr Sp Tech* 46:64–75
- Lei MF, Lin DY, Yang WC, Shi CH, Peng LM, Huang J (2016) Model test to investigate failure mechanism and loading characteristics of shallow-bias tunnels with small clear distance. *J Cent South Univ* 23:3312–3321
- Li DY, Li XB, Li CC, Huang BR, Gong FQ, Zhang W (2009) Case studies of groundwater flow into tunnels and an innovative water-gathering system for water drainage. *Tunn Undergr Sp Tech* 24:260–268
- Li SC, Zhou ZQ, Li LP, Xu ZH, Zhang QQ, Shi SS (2013) Risk assessment of water inrush in karst tunnels based on attribute synthetic evaluation system. *Tunn Undergr Sp Tech* 38:50–58
- Li SC, Lin P, Xu ZH, Li LP, He SJ, Zhao SL, Huang X (2017a) Innovative method for the integral sliding stability analysis of filling media in karst caves and its applications in engineering. *Int J Geomech* 17:04017109
- Li XZ, Zhang PX, He ZC, Huang Z, Cheng ML, Guo L (2017b) Identification of geological structure which induced heavy water and mud inrush in tunnel excavation: a case study on Lingjiao tunnel. *Tunn Undergr Sp Tech* 69:203–208
- Li SC, Gao CL, Zhou ZQ, Li LP, Wang MX, Yuan YC, Wang J (2019) Analysis on the precursor information of water inrush in karst tunnels: a true triaxial model test study. *Rock Mech Rock Eng* 52:373–384
- Ma D, Miao XX, Bai HB, Huang JH, Pu H, Wu Y, Zhang GM, Li JW (2016) Effect of mining on shear sidewall groundwater inrush hazard caused by seepage instability of the penetrated karst collapse pillar. *Nat Hazards* 82:73–93
- Nam SW, Bobet A (2006) Liner stresses in deep tunnels below the water table [J]. *Tunn Undergr Space Technol* 21(6):626–635
- Tian QY, Zhang JT, Zhang YL (2018) Similar simulation experiment of expressway tunnel in karst area. *Constr Build Mater* 176:1–13
- Wang XY, Tan ZS, Wang MS, Zhang M, Huang FM (2008) Theoretical and experimental study of external water pressure on tunnel lining in controlled drainage under high water level. *Tunn Undergr Sp Tech* 23:552–560
- Wu J, Li SC, Xu ZH, Huang X, Xue YG, Wang ZC, Li LP (2017) Flow characteristics and escape-route optimization after water inrush in a backward-excavated karst tunnel. *Int J Geomech* 17:04016096
- Xiao XX, Xu M, Ding QZ, Kang XB, Xia Q, Du F (2018) Experimental study investigating deformation behavior in land overlying a karst cave caused by groundwater level changes. *Environ Earth Sci* 77:1–11
- Yuan Y, Jiang X, Lee CF (2000) Tunnel waterproofing practices in China. *Tunn Undergr Sp Tech* 15:227–233
- Yang GC, Wang XH, Wang XG, Cao YG (2016) Analyses of seepage problems in a subsea tunnel considering effects of grouting and lining structure. *Mar Georesour Geotech* 34:65–70
- Ye F, Gou CF, Sun HD, Liu YP (2014) Model test study on effective ratio of segment transverse bending rigidity of shield tunnel. *Tunn Undergr Sp Tech* 41:193–205
- Zhao Y, Tian SM (2019) Data statistics of railway tunnel in China up to the end of 2018. *Tunn Constr* 39:324–335
- Zhao Y, Tian SM, Sun Y (2017) Development and planning of high-speed railway tunnels in china. *Tunn Constr* 37:11–17

Publisher's Note Springer Nature remains neutral with regard to jurisdictional claims in published maps and institutional affiliations.